Peltier Cooling and Onsager Reciprocity in Ferromagnetic Thin Films

A. D. Avery and B. L. Zink

Department of Physics and Astronomy, University of Denver, Denver, Colorado 80208, USA

(Received 22 March 2013; published 17 September 2013)

We present direct measurements of the Peltier effect as a function of temperature from 77 to 325 K in Ni, $Ni_{80}Fe_{20}$, and Fe thin films made using a suspended Si-N membrane structure. Measurement of the Seebeck effect in the same films allows us to directly test predictions of Onsager reciprocity between the Peltier and Seebeck effects. The Peltier coefficient Π is negative for both Ni and $Ni_{80}Fe_{20}$ films and positive for the Fe film. The Fe film also exhibits a peak associated with the magnon drag Peltier effect. The observation of magnon drag in the Fe film verifies that the coupling between the phonon, magnon, and electron systems in the film is the same whether driven by heat current or charge current. The excellent agreement between Π values predicted using the experimentally determined Seebeck coefficient for these films and measured values offers direct experimental confirmation of the Onsager reciprocity between these thermoelectric effects in ferromagnetic thin films near room temperature.

DOI: 10.1103/PhysRevLett.111.126602 PACS numbers: 72.15.Jf, 72.25.Ba, 73.50.Jt, 73.50.Lw

The Peltier effect and the Seebeck effect are the two most fundamental thermoelectric phenomena and a primary focus in the emerging field of spin caloritronics [1,2]. This field focuses on coupling of heat, charge, and spin in magnetic materials and includes recent studies of field-dependent Seebeck effects in magnetic multilayers, nanostructures, and tunnel junctions [3–8], and the spin analogs of Peltier and Seebeck effects in ferromagnetic metal structures and tunneling devices and their use for the thermal generation of spin injection and pure spin currents [9–12]. In the Seebeck effect, a material develops a current or voltage in response to a thermal gradient. Conversely, the Peltier effect is a temperature difference developed across a material in response to an applied current. The importance of both effects stems from their role in applications ranging from thermoelectric energy generation [13] to spot cooling of integrated circuits [14,15].

Onsager reciprocity [16], the main result in the thermodynamics of nonequilibrium processes, assumes microscopic reversibility applied to fluctuations and relates generalized thermodynamic forces with generalized currents. The general mathematical expression linking forces and currents is $\dot{q}_i = \Sigma_{j=1}^{N} L_{ij} X_j$, where $\dot{q}$ is a generalized current, X_J is a generalized force, and L_{ij} is the coefficient relating the two. Onsager reciprocity applies to the off-diagonal elements in the L_{ij} matrix such that $L_{ij} = L_{ji}$. This relation is expected to hold in systems that maintain time-reversal symmetry and has been demonstrated for a wide variety of physical phenomena [17], including thermoelectric effects [18]. Applying these conditions to the charge and heat flow through a material yields a system of equations

$$\begin{pmatrix} \vec{J} \\ \vec{Q} \end{pmatrix} = \sigma \begin{pmatrix} 1 & \alpha \\ \Pi & k/\sigma \end{pmatrix} \begin{pmatrix} \nabla V \\ -\nabla T \end{pmatrix}, \tag{1}$$

where $\vec{Q}$ is the heat current density, $\vec{J}$ is the electrical current density, σ is the electrical conductivity, and k is the thermal conductivity [19,20]. The off-diagonal coefficient elements are the Seebeck coefficient (α) and the Peltier coefficient (Π), and Onsager reciprocity predicts $\Pi = \alpha T$ [20].

In the Seebeck effect, a temperature difference maintained across a sample excites phonons and electrons that transport energy through the film. When no steady-state current can flow through the sample, charge flows only until the electric field balances the heat flow through the film. The thermopower is the resulting voltage drop, and the Seebeck coefficient $\alpha = \Delta V/\Delta T$. In magnetic thin films spin waves, or magnons, can increase ΔV by transporting additional energy from the phonons to the electrons. The increase in α through magnons is known as magnon drag [21] and is analogous to phonon drag that is usually observed at low temperatures in bulk metals such as copper [22]. Though rarely explored experimentally, Costache *et al.* recently reported magnon drag effects in narrow Ni-Fe wires [23] and we observed magnon drag in Fe films [24]. The large magnon drag peak in Fe is normally explained by the presence of both spin-up and spin-down $3d$ bands at the Fermi level in Fe. This allows potentially larger electron-magnon interactions than in Ni where the spin-down d band falls below the Fermi level and the s band dominates transport [21].

Compared to the substantial body of work on the Seebeck effect, few experiments have explored the Peltier effect and fewer still have offered verification of Onsager reciprocity by measuring α and Π on the same sample. Measurements of α are more straightforward and do not require the highly sensitive thermometry usually necessary to measure Π, a situation made even more challenging for thermal measurements in scaled-down geometries such as thin films [24–27]. Among the few

measurements of Π to be found in the literature are studies of simple metals mostly made at a single temperature reviewed by Miller [17], work mostly focused on semiconductors or assembled thermoelectric modules [28–31], a study of a metallic thermopile [32], and investigation of giant magnetoresistive multilayers with the current perpendicular to plane [33]. There is also an experiment that explored the magnon drag component in Ni-Cu and Ni-Fe alloys below 4.2 K, observing a reduction in Π after quenching magnons using a large applied external magnetic field [34]. Of these previous studies, only the review by Miller and the recent work by Garrido and Casanovas present experimental tests of Onsager reciprocity between Π and α [31,35]. These show Onsager reciprocity to be valid within considerable experimental error bars, though there are some reports of possible violation of reciprocity in underdoped cuprates [36]. To our knowledge there are no previous experiments exploring the Peltier effect in Ni, Ni-Fe, and Fe thin films. Furthermore we know of no previous experiments on Onsager reciprocity in samples that exhibit magnon drag, which would offer insight into which couplings between excitations maintain time-reversal symmetry, even in the presence of external magnetic fields.

In this Letter, we present experimental measurements of the Peltier effect. Comparing the results from the Peltier measurements and predictions of Π using previously measured α allows us to test the Onsager reciprocal relation directly as well as probe the coupling between thermally excited electrons, phonons, and magnons in ferromagnetic thin films. We first describe the suspended Si-N thermal isolation platforms which enable sensitive thermal and electrical transport measurements. Next we present our methodology for measuring Π. One of the major advantages of our technique is the flexibility to apply either a charge current or heat current through a thin film and monitor the resulting temperature or potential difference generated as a consequence of the Seebeck and Peltier effects on the same film. Finally, we present results for 20 nm thick Ni, permalloy (Ni-Fe), and Fe thin films measured from 77 to 325 K and discuss the validity of the Onsager reciprocity between Π and α.

We measured Π on 20 nm thick Ni and Ni-Fe films supported by 500 nm thick suspended low-stress Si-N membranes. These thermal isolation platforms are from the same wafer as those previously used to measure the planar Nernst effect, magnetic field dependent thermopower, and anisotropic magnetoresistance [26,27]. We deposited the Ni and Ni-Fe films via rf sputtering. Each thermal isolation platform has two islands patterned with a thermometer and heater. The sample film and its supporting bridge provide the only thermal path between the two islands. Eight legs connect the platform to the frame and suspend the platform to eliminate contact with the large thermal mass of the Si frame. Figure 1(b) is a scanning electron microscope (SEM) image showing an example thermal isolation platform and the surrounding Si frame. Figure 1(a) is a close-up of the platform that highlights the thermometry and illustrates the current path through the film. There is an additional thermometer on the Si frame for monitoring the bath temperature throughout the experiment. We present detailed steps for platform fabrication in a previous publication [26]. Our experimental setup using a sample-in-vacuum liquid nitrogen cryostat limits our temperature range to 77–325 K.

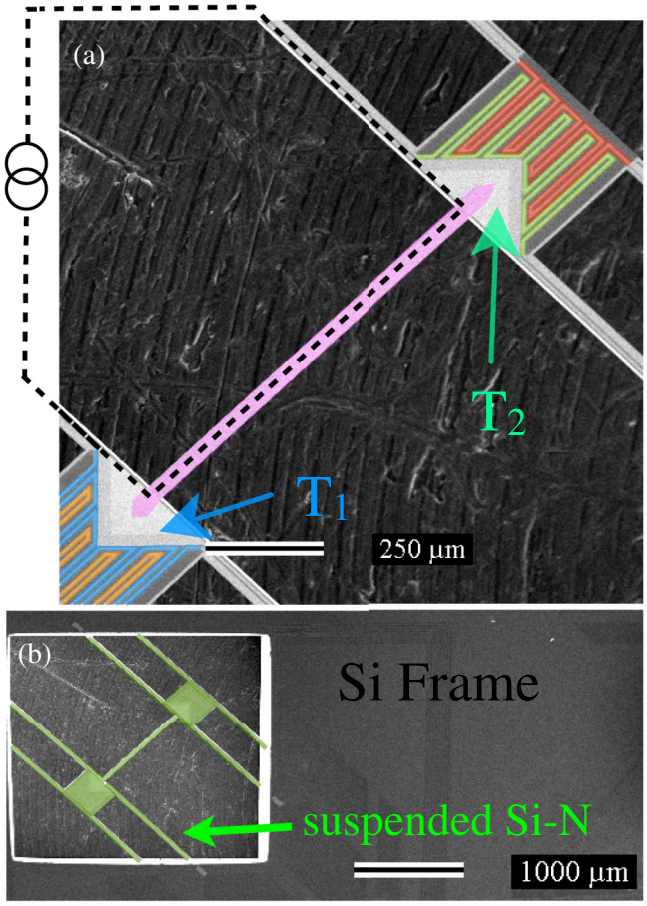

FIG. 1 (color online). SEM micrograph with false color highlights (heaters, red and orange; thermometers, blue and green; sample, pink) shows the platform used to measure the Peltier effect. (a) The two suspended islands at temperatures T_1 and T_2 with heaters, thermometers, and electrical leads visible. The dashed line indicates the current path through the film. (b) A larger view shows the Si-N membrane platform (highlighted in green) and the surrounding Si frame.

To develop expressions for the Joule power (P_J) and the Peltier power (P_Π) dissipated in the film, we start with a system of steady-state heat flow equations for the thermal model illustrated in Fig. 2(a),

$$P_J + P_\Pi = K_L(T_1 - T_0) + K_B(T_1 - T_2), \quad (2)$$

$$P_J - P_\Pi = K_L(T_2 - T_0) + K_B(T_2 - T_1). \quad (3)$$

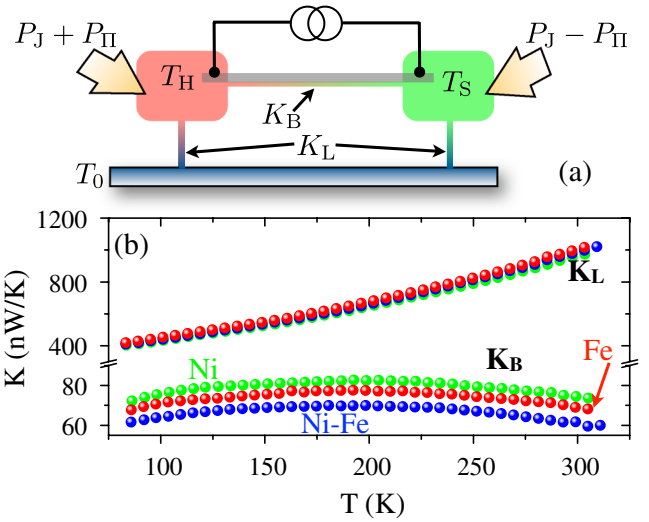

FIG. 2 (color online). (a) Thermal model for heat flow due to the Peltier and Joule effects in the thermal platform. (b) K_L and K_B vs T for 20 nm Ni, Ni-Fe, and Fe films supported by Si-N membrane platforms. K_L is thermal conductance for the legs connected to the Si frame and K_B is thermal conductance through the film and the supporting Si-N bridge connecting the islands. Estimated error on K_L and K_B is 1% or less.

In these equations, T_1, T_2, and T_0 are the temperatures on either end of the film and the Si frame, K_L is thermal conductance of the legs, and K_B is the thermal conductance of the sample film and its supporting Si-N bridge. Solving for P_J and P_Π gives

$$P_J = \frac{1}{2}K_L(\Delta T_1 + \Delta T_2), \tag{4}$$

$$P_\Pi = (K_B + \frac{1}{2}K_L)\Delta T_f. \tag{5}$$

Here $\Delta T_1 = T_1 - T_0$, $\Delta T_2 = T_2 - T_0$, and $\Delta T_f = T_1 - T_2 = \Delta T_1 - \Delta T_2$. We see that P_J is a function of K_L and the temperature differences generated along the legs. P_Π depends instead on K_B and ΔT_f.

We begin a Peltier experiment by calibrating each of the three experimental thermometers. At each T_0, we regulate the temperature of the bath and measure all three resistances with no external applied current in the sample. We perform a separate calibration for each thermometer on each thermal isolation platform during every experiment. In this way, we ensure the most accurate determination of T_0, T_1, and T_2 using their respective $T(R)$ functions. We then apply a series of currents from negative to positive and record T_1 and T_2. Next, we determine P_Π, the power generated by the Peltier effect, using Eq. (5) and measured values for K_B, K_L, T_1, T_2, and T_0. Once P_Π is determined for each I, $P_\Pi = \Pi I$ allows determination of Π via a linear fit of P_Π vs I. We also monitor the frame thermometer for temperature stability at each T_0. Finally, we measure the voltage drop across the film as a function of I to determine the film resistance.

The total temperature difference at the hot end of the film, $\Delta T_{\text{hot}} = \Delta T_J + \Delta T_\Pi$, is a sum of ΔT from the Joule effect and the Peltier effect. Reversing the current causes the Peltier effect to switch from liberating heat to absorbing heat. However, the Joule effect still adds heat, and the temperature difference becomes $\Delta T_{\text{cold}} = \Delta T_J - \Delta T_\Pi$. We can take advantage of the symmetry of the Joule effect to determine its contribution to the total ΔT. Thus, adding ΔT_{cold} and ΔT_{hot} developed at opposite ends of a film gives $2\Delta T_J$. Subtracting the ΔT_J contribution from ΔT_{hot} gives $+\Delta T_\Pi$ and subtracting from ΔT_{cold} gives $-\Delta T_\Pi$.

Figures 3(a) and 3(b) show ΔT_1 and ΔT_2, respectively, for a Ni film as a function of applied I from -60 to $+60$ μA in 10 μA increments. With no analysis or interpretation, evidence of the Peltier effect is clear from the asymmetry of the total measured ΔT around $I = 0$. If only Joule heating occurs, ΔT should be strictly $\propto I^2$. In Fig. 3(a), $2\Delta T_J = \Delta T_1(I = 60\ \mu\text{A}) - \Delta T_1(I = -60\ \mu\text{A})$, and in Fig. 3(b), $2\Delta T_J = \Delta T_2(I = 60\ \mu\text{A}) - \Delta T_2(I = -60\ \mu\text{A})$. Subtracting this symmetric component isolates ΔT_Π, which is linear and symmetric about $I = 0$ μA. For positive (negative) I, T_1 is cooler (warmer). Of course the converse is true for T_2. The increase in temperature generated through both the Joule and Peltier effects compared to the reference temperature of the experiment is 3.5% at 77 K and less than 1% at 300 K and is well within a linear regime.

To determine the power dissipated by the Joule effect and the Peltier effect resulting in the observed ΔT_J and

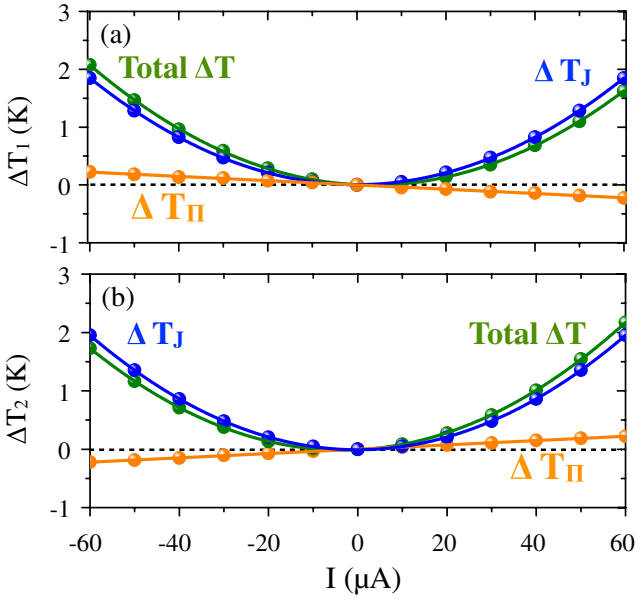

FIG. 3 (color online). (a) $\Delta T_1 = T_1 - T_0$ and (b) $\Delta T_2 = T_2 - T_0$ as a function of applied I through a 20 nm thick Ni film. Total ΔT is in green, symmetric in current contribution from Joule heating ΔT_J is in blue, and ΔT_Π is orange. Estimated error on each total $\Delta T \sim 70$ mK.

ΔT_Π, we substitute the experimentally determined T_1, T_2, and T_0 values from this experiment and K_L and K_B values determined in earlier measurements of the Ni-Fe film and similar Ni and Fe films from the same wafer into Eqs. (4) and (5). For a detailed explanation of our technique for measuring K_L and K_B, see Ref. [37]. Figure 2(b) shows thermal conductance as a function of temperature for 20 nm thick Ni, Fe, and Ni-Fe films supported by Si-N membrane structures. K_L represents the conductance through the suspension legs connecting the thermal isolation platform to the Si frame and through the metallic wires running along them. K_B is the total thermal conductance contributed by the Si-N bridge plus a 20 nm thick film deposited on the bridge. The temperature dependence and magnitude of the thermal conductance displayed in Fig. 2(b) are comparable to previous measurements of K conducted on similar films as expected [25,38].

Figure 4(a) presents α as a function of T for 20 nm Ni-Fe, Ni, and Fe films. The temperature dependence of α for all three films is similar to previous measurements of ferromagnetic films performed on earlier versions of these thermal isolation platforms [24]. Note that, for both Seebeck and Peltier experiments, there is a small contribution (either a thermovoltage or a temperature drop) from the thin film molybdenum electrical leads that connect the sample to the bond pads on the Si frame at T_0. In other words, thermoelectric values measured here are relative, rather than absolute [39]. Figure 4(b) shows Π measured as a function of average sample $T = T_0 + (\Delta T_f/2)$ for the exact same Ni-Fe film and for Ni and Fe films grown on the same wafer in very close proximity to those used for α measurements. Each data point is determined from the slope of a linear fit to P_Π vs I, as shown in the inset of Fig. 4 for a base temperature of 276 K. The similarities in Π between Ni and Ni-Fe as well as the differences between these films and the Fe film are immediately apparent, with a negative Π in Ni and Ni-Fe and positive Π for Fe, as expected from the sign of the $\Pi = \alpha T$ prediction.

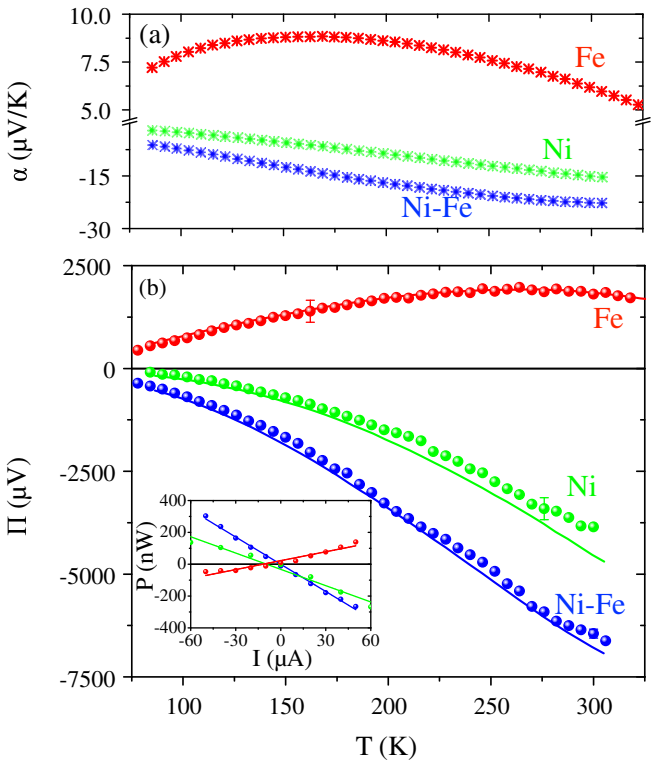

FIG. 4 (color online). (a) α as a function of temperature for a Ni film (green), a Ni-Fe film (blue), and a Fe film (red), all 20 nm thick. (b) Π as a function of temperature for the Ni-Fe (blue) film as well as a Ni film (green) and a 20 nm Fe film (red) from the same wafer. Predicted Π values from $\Pi = \alpha T$ are represented by solid lines. Inset plot displays the power generated by the Peltier effect, P_Π versus current at 276 K. The slope of the linear fit to the P_Π versus I plot at each reference temperature gives the Peltier coefficient Π.

The Π values predicted from Onsager reciprocity, calculated using $\Pi = \alpha T$ using α from Fig. 4(a), are represented in Fig. 4(b) by solid lines. Π for all three films is in excellent agreement with predicted values. The additional thermopower indicated by the peak in Fe α originates from magnon drag. This peak appears in Π as well. This confirms that Onsager reciprocity applies not only to the electrons and phonons, but to the interaction between these excitations and magnons as well.

Finally, we comment on magnetic field dependence of the α and Π measurements. We have previously observed a small dependence of α on applied magnetic field in these Ni and Ni-Fe films that arises from the same spin-dependent scattering mechanism that drives the anisotropic magnetoresistance effect in ferromagnetic metal films [26] (no change in α was detected in the Fe film with H up to $\sim$1700 Oe). Onsager reciprocity then suggests a similar field dependence in Π, though perhaps with opposite sign due to the antisymmetry in magnetic field implicit in time-reversal symmetry. Though we searched for a field dependence in Π, we did not observe any change in Π with field within our current measurement accuracy. Since detecting the field dependence of α was already challenging, new and more sensitive techniques will be required for a rigorous test of the effect of field.

In summary, we have measured the Peltier coefficient in Ni, Ni-Fe, and Fe thin films. Ni and Ni-Fe films displayed a negative $\Pi(T)$ while the Fe film $\Pi(T)$ was positive as expected from previously measured $\alpha(T)$ values. In contrast to the Ni and Ni-Fe films, the Fe film exhibited a peak associated with the Peltier effect magnon drag. $\Pi(T)$ measured for all three films was in excellent agreement with the prediction of Onsager reciprocity. This experimentally confirms the microscopic time reversibility between the Peltier and Seebeck effects. Finally, the observation of magnon drag in the Fe film confirms the microscopic time-reversal symmetry of magnon drag. This verifies that the coupling between the phonon, magnon, and

electron systems in the film is equal and reversible whether driven by a heat current or with a charge current.

We gratefully acknowledge support from the NSF CAREER Grant No. DMR-0847796. We also thank M. R. Pufall of the NIST Boulder Magnetics Group for deposition of the films and many helpful discussions, J. Beall, G. Hilton, D. Schmidt, and A. Fox for fabrication advice and assistance, and J. Underwood, S. Mason, and D. Bassett for assistance in the laboratory.

[1] G. E. W. Bauer, A. H. MacDonald, and S. Maekawa, Solid State Commun. **150**, 459 (2010).
[2] G. E. W. Bauer, E. Saitoh, and B. J. van Wees, Nat. Mater. **11**, 391 (2012).
[3] J. Shi, S. S. P. Parkin, L. Xing, and M. B. Salamon, J. Magn. Magn. Mater. **125**, L251 (1993).
[4] L. Gravier, S. Serrano-Guisan, F. Reuse, and J.-P. Ansermet, Phys. Rev. B **73**, 024419 (2006).
[5] M. Walter, J. Walowski, V. Zbarsky, M. Munzenberg, M. Schafers, D. Ebke, G. Reiss, A. Thomas, P. Peretzki, M. Seibt, J. S. Moodera, M. Czerner, M. Bachmann, and C. Heiliger, Nat. Mater. **10**, 742 (2011).
[6] N. Liebing, S. Serrano-Guisan, K. Rott, G. Reiss, J. Langer, B. Ocker, and H. W. Schumacher, Phys. Rev. Lett. **107**, 177201 (2011).
[7] B. Scharf, A. Matos-Abiague, I. Žutić, and J. Fabian, Phys. Rev. B **85**, 085208 (2012).
[8] A. von Bieren, F. Brandl, D. Grundler, and J.-P. Ansermet, Appl. Phys. Lett. **102**, 052408 (2013).
[9] A. Slachter, F. L. Bakker, J.-P. Adam, and B. J. van Wees, Nat. Phys. **6**, 879 (2010).
[10] F. L. Bakker, A. Slachter, J.-P. Adam, and B. J. van Wees, Phys. Rev. Lett. **105**, 136601 (2010).
[11] J.-C. Le Breton, S. Sharma, H. Saito, S. Yuasa, and R. Jansen, Nature (London) **475**, 82 (2011).
[12] J. Flipse, F. L. Bakker, A. Slachter, F. K. Dejene, and B. J. van Wees, Nat. Nanotechnol. **7**, 166 (2012).
[13] L. E. Bell, Science **321**, 1457 (2008).
[14] I. Chowdhury, R. Prasher, K. Lofgreen, G. Chrysler, S. Narasimhan, R. Mahajan, D. Koester, R. Alley, and R. Venkatasubramanian, Nat. Nanotechnol. **4**, 235 (2009).
[15] A. Majumdar, Nat. Nanotechnol. **4**, 214 (2009).
[16] L. Onsager, Phys. Rev. **37**, 405 (1931).
[17] D. G. Miller, Chem. Rev. **60**, 15 (1960).
[18] H. B. Callen, Phys. Rev. **73**, 1349 (1948).
[19] *Spin Current*, edited by S. Maekawa, S. Velnzuela, E. Saitoh, and T. Kimura (Oxford University Press, New York, 2012).
[20] J. M. Ziman, *Electrons and Phonons* (Oxford University, London, 1960).
[21] F. J. Blatt, D. J. Flood, V. Rowe, P. A. Schroeder, and J. E. Cox, Phys. Rev. Lett. **18**, 395 (1967).
[22] I. Weinberg, Phys. Rev. **146**, 486 (1966).
[23] M. V. Costache, G. Bridoux, I. Neumann, and S. O. Valenzuela, Nat. Mater. **11**, 199 (2012).
[24] A. D. Avery, R. Sultan, D. Bassett, D. Wei, and B. L. Zink, Phys. Rev. B **83**, 100401 (2011).
[25] B. L. Zink, A. D. Avery, R. Sultan, D. Bassett, and M. Pufall, Solid State Commun. **150**, 514 (2010).
[26] A. D. Avery, M. R. Pufall, and B. L. Zink, Phys. Rev. B **86**, 184408 (2012).
[27] A. D. Avery, M. R. Pufall, and B. L. Zink, Phys. Rev. Lett. **109**, 196602 (2012).
[28] A. T. Fiory and B. Serin, Phys. Rev. Lett. **16**, 308 (1966).
[29] H. Zou, D. Rowe, and S. Williams, Thin Solid Films **408**, 270 (2002).
[30] H. Straube, J.-M. Wagner, and O. Breitenstein, Appl. Phys. Lett. **95**, 052107 (2009).
[31] J. Garrido and A. Casanovas, J. Electron. Mater. **41**, 1990 (2012).
[32] J. Jimenez, E. Rojas, and M. Zamora, J. Appl. Phys. **56**, 3250 (1984).
[33] A. Fukushima, H. Kubota, A. Yamamoto, Y. Suzuki, and S. Yuasa, IEEE Trans. Magn. **41**, 2571 (2005).
[34] G. N. Grannemann and L. Berger, Phys. Rev. B **13**, 2072 (1976).
[35] J. Garrido, J. Phys. Condens. Matter **21**, 155802 (2009).
[36] C. M. Varma, V. M. Yakovenko, and A. Kapitulnik, arXiv:1007.1215v2.
[37] R. Sultan, A. D. Avery, G. Stiehl, and B. L. Zink, J. Appl. Phys. **105**, 043501 (2009).
[38] A. D. Avery, Ph.D. thesis, University of Denver, 2013.
[39] First results from ongoing experiments measuring relative α along with thermal and electrical conductivity as a function of film thickness, which allows calculation of the absolute sample α, suggest the leads contribute much less than 10% of the total signal. This indicates α is strongly reduced in Mo thin films compared to bulk, as we have previously observed for other thin film materials.